2021-01-0456 Published 06 Apr 2021

Assessment of In-Cylinder Thermal Barrier Coatings over a Full Vehicle Drive Cycle

George Koutsakis University of Wisconsin-Madison

Scott Miles John Deere Power Systems

Jaal Ghandhi University of Wisconsin-Madison

Citation: Koutsakis, G., Miles, S., and Ghandhi, J., "Assessment of In-Cylinder Thermal Barrier Coatings over a Full Vehicle Drive Cycle," SAE Technical Paper 2021-01-0456, 2021, doi:10.4271/2021-01-0456.

Abstract

In-cylinder thermal barrier coatings (TBCs) have the capability to reduce fuel consumption by reducing wall heat transfer and to increase exhaust enthalpy. Low thermal conductivity, low volumetric heat capacity thermal barrier coatings tend to reduce the gas-wall temperature difference, the driving potential for heat transfer from the gas to the combustion chamber surfaces. This paper presents a coupling between an analytical methodology for multi-layer coated wall surface temperature prediction with a fully calibrated production model in a commercial system-level simulation software package (GT-Power). The wall surface temperature at each time step was calculated efficiently by convolving the engine wall response function with the time-varying surface boundary condition, *i. e.*, in-cylinder heat flux and coolant temperature. This tool allows the wall to be treated either as spatially uniform with one set of properties, or with independent head/piston/liner components. Steady state results are presented for five modern, engine-specific coating architectures selected from the literature. The coating performance, on a system-level basis, was found to be engine-condition dependent. The optimum material for one performance parameter may not provide any benefit to another. To comprehensively compare TBCs relative to the uncoated baseline, a full transient drive cycle simulation was performed for two coatings using the 20-minute certification Non-Road Transient Cycle (NRTC). Experimental boundary conditions along with ECU data were provided from production engine test cell data. A reduction of in-cylinder heat transfer and fuel consumption was found for both coatings, while exhaust enthalpy was increased by 0.5% in spite of the fuel mass saving. For a piston-coated scenario, a maximum of 1.5% reduction in fuel consumption and consequently a similar level of brake specific CO_2 reduction was realized over the drive cycle, depending on the coating architecture.

Introduction

The desire to reduce fuel energy rejected to the environment motivates the need for a better understanding of engine heat transfer. A pathway to achieve higher efficiency is to reduce the heat transfer losses to the combustion chamber walls by depositing insulating coatings on the combustion chamber surfaces. A recent trend in the automotive industry is to downsize and downspeed internal combustion engines. Reducing combustion chamber volume results in higher surface area-to-volume ratio, but boosting to recover power leads to higher pressures and temperatures, which promotes heat transfer losses.

The choice of optimal in-cylinder coating materials for internal combustion engines is not clear. Engines can be used over a wide range of speeds and loads, thus the optimum material for one application may not be the most favorable for another. Furthermore, a coating material that optimizes one performance parameter may adversely affect another performance parameter. For instance, if a coated engine is operated at high loads, *i.e.*, higher wall surface temperatures, the heat transfer during combustion and power stroke might be lower compared to the baseline, but the higher surface temperatures reduce air mass flow and consequently engine power output.

In-cylinder thermal insulation has a long history for internal combustion engines. A recent state-of-the-art literature review [1], provides a historical evolution of TBC technology starting from 1970s up to the current day. It focuses on the conflicting nature of the engine performance and emission results with respect to the thermal barrier coating characteristics, *e.g.* material (thermal/radiative) properties, thickness, porosity and surface roughness. Apart from the coating material properties, it discusses how the gas-wall interface characteristics (*e.g.* velocity gradient, flame distribution, local near wall air-fuel mixture composition and radiative heat transfer) affected the earlier engine performance studies. Additional literature for CI engines can also be also found in [2, 3, 4]. A wide variety of steady state performance studies utilizing finite difference schemes for in-cylinder heat transfer have been recently reported [5, 6, 7, 8, 9, 10, 11]. However, drive cycle engine simulations with in-cylinder

TBCs have not been widely reported in the engine literature for reasons that will be discussed later.

Five unique wall coating architectures, specifically designed for reciprocating internal combustion engine applications, with various thermal properties and thickness were collected from the modern thermal barrier coating literature and will be investigated in this paper. All of these coatings have been validated experimentally and showed favorable results. Coating #1: A plasma-sprayed gadolinium zirconate (GdZr) deposited on a piston surface extended the low-load (or misfire) operating envelope of a gasoline homogeneous charge compression ignition (HCCI) engine [12]. The combustion efficiency was increased by 1.5% and, the indicated thermal efficiency by 5%, relative to an uncoated baseline. Lower unburned hydrocarbons (uHC) and carbon monoxide (CO) emissions indicated faster near-wall chemical kinetics. Coating #2: A traditional atmospheric plasma-sprayed yttria-stabilized zirconia (YSZ) coating with gradient and bond coats [13] was tested over a range of high-output diesel operating conditions. Various roughness and thickness were applied to the piston surface. Most of the rough (as-coated) pistons showed an increase in fuel consumption, but a smooth version showed an increase of gross indicated thermal efficiency up to 3.5% (relative to the uncoated case). Coating # 3: Reliable operation in a spark-ignited engine environment was demonstrated using a high volume low pressure (HVLP) coating method [14]. These coatings include aluminosilicate particles dispersed in an organic polysilazane or metal phosphate binder [15]. Coating #4: A production silica reinforced porous anodized aluminum (SiRPA) coating developed by Toyota [11] that showed lower fuel consumption and higher cold-start efficiency in diesel engine experiments [8, 16]. An energy balance revealed a reduction in cooling requirements and, thus, an increase in brake power and exhaust loss. Coating #5: Several coating structures were developed under the European project EAGLE [17]. The coatings were designed to operate in a light duty, lean-burn spark ignited gasoline engine environment. The coating surface temperature swing was measured via the laser-induced phosphorescence technique in an optical engine setup. The most promising coating (case E, which was selected in this study for evaluation) reached a temperature swing of 100°C. A metal engine with identical geometry was used to measure performance and emissions. The same coating also showed lower indicated thermal efficiency at low load conditions, however less cooling losses, better combustion efficiency and higher heat release rates were reported [18]. Even though this is a multi-layer coating, only effective properties of a single layer were provided [19].

Surface roughness may play an important role in the combustion chamber heat transfer. There is evidence that roughness influences near-wall air-fuel mixing and combustion, which may explain results that differ from what would have been expected by smooth higher temperature walls [20, 21, 22, 23, 24]. Increased surface roughness provides more effective area and can increase near-wall turbulence. Additionally, the air-fuel mixing process can be affected, which in turn, affects chemistry. Machined metal combustion chamber walls have surface roughness in the order of Ra of 1 μm. The SiRPA coating was reported to have surface roughness Ra 3-5 μm, which was due to the uneven alumina growth of the anodizing process [25]. Traditional thermal barrier coatings deposited via atmospheric plasma spray techniques can have Ra more than 10 μm [26, 13]. The lack of quantitative information on the effect of surface roughness on heat transfer prevents it from being included in these calculations.

Finite difference techniques have been widely used in the literature to predict the wall surface temperature of combustion chambers. There are two main drawbacks associated with the finite difference approach versus analytical methods. First, the time step in a finite difference approach must be chosen to ensure numerical stability, and second and most important, all the nodal temperatures are computed and stored for each time step even though only the surface node is the only output of interest explicitly for providing boundary conditions in engine simulation. In commercial simulation codes the time step is dictated by the combustion-fluid solver, which is chosen to ensure numerical stability by satisfying the Courant condition. However, the finite difference heat conduction solver has its own stability requirements. Thin coatings have short time scales that require high density nodal discretization near the surface to guarantee numerical stability and accuracy, which reduces computational efficiency.

The objective of this work is to implement the conduction heat transfer methodology developed for multi-layer walls from previous works [2, 3] in a commercial simulation software in order to evaluate thermal barrier coatings performance in a system-level simulation. The proposed tool was used for steady-state and transient drive cycle calculations to assess the five coating architectures from the modern literature discussed above.

Wall Temperature from Heat Flux

Consider 1-D heat flow in a plane wall with overall thickness L and constant thermophysical properties within each layer. The governing heat diffusion equation is

$$k\frac{\partial^2 t}{\partial x^2} = \rho c\frac{\partial t}{\partial \theta} \tag{1}$$

where t is temperature, θ is time, k and ρc are thermal conductivity and volumetric heat capacity, respectively. The $x = 0$ location, see Fig. 1, represents the combustion chamber surface where a time-varying heat flux, $\dot{q}''(\theta)$, is imposed.

$$-k\left.\frac{\partial t}{\partial x}\right|_{x=0} = \dot{q}''(\theta) = f(\theta) \tag{2}$$

The applied heat flux could be aperiodic in transient operation of a reciprocating engine. During the initial warm-up or even during large engine load changes the backside wall temperature may also change significantly. For the backside condition at $x = L$ the coolant or oil temperature is used, and allowed to vary as a prescribed function of time

$$t_c(\theta) = f(\theta) \tag{3}$$

FIGURE 1 Illustration of an 1-D multi-layer engine wall. Both boundary conditions, *i.e.* heat flux on the combustion chamber gas-side and temperature on the coolant side, are prescribed functions of time.

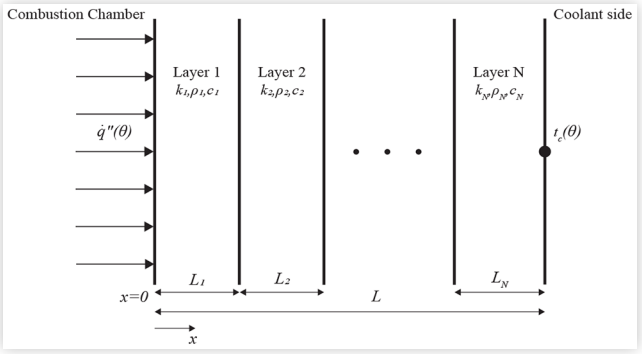

The problem is formulated with linear and homogeneous boundary conditions, constant thermophysical properties and therefore the principle of superposition can be applied to the heat diffusion equation. The transient problem is divided into two sub-problems, one for each of the boundary conditions. Their superposition comprises the general solution. Inversion from the Laplace domain is performed via the residue theorem. The full wall temperature solution, given the arbitrary combustion heat flux and backside temperature history, for the time of interest θ_n is given as

$$t_o\left(\theta_n\right)=\sum_{i=0}^{n}X\left(\theta_n-\theta_i\right)\cdot\Delta\dot{q}''_{o,i}+\sum_{i=0}^{n}Y\left(\theta_n-\theta_i\right)\cdot\Delta t_{N,i} \quad (4)$$

where $X(\theta_n-\theta_i)$ is the response function of the combustion surface due to the heat flux changes, and $Y(\theta_n-\theta_i)$ is the response function of the combustion surface due to the backside (coolant/oil) temperature changes. The X and Y response functions describe how the multi-layer structure absorbs and releases heat over a finite/prolonged period of time. The terms $\Delta\dot{q}''_{o,i}\equiv\left(\dot{q}''_{o,i}-\dot{q}''_{o,i-1}\right)$ and $\Delta t_{N,i}\equiv(t_{N,i}-t_{N,i-1})$ are the discretized combustion heat flux steps and backside temperature steps, respectively. A full discussion of the response functions X and Y is given in [2].

This one-dimensional analytical technique for calculating wall surface temperature for long-time problems with constant thermophysical properties is more efficient than Euler, Crank-Nicolson and other classical finite difference methods for the following reasons:

1. The solution is exact, however accuracy is dependent on the discretized temporal boundary condition, as it is for the finite difference solution
2. There is no critical time step
3. The internal temperature distribution is not calculated
4. All the necessary information is contained in the response function, which is a function of time step size and wall material properties and can, therefore, be calculated *a priori*

For further details about the solution method, see [2, 3].

TABLE 1 John Deere 4045HFC04 engine geometry

Number of cylinders	4
Displacement volume	4.5 L
Stroke	127 mm
Bore	106.5 mm
Connecting Rod	203 mm
Compression Ratio	17.0:1
Firing order	1-3-4-2

Engine Model Specifications

The coated wall temperature methodology was implemented in GT-Power [27]. The production John Deere 4045 engine, see Table 1, was modeled. All major subsystems in this model use bench data or have been suitably calibrated, including the head flow, EGR valve, exhaust throttle, turbocharger, wastegate, fuel rate of injection profiles, and combustion parameters. Input settings were extracted from the production ECU calibration, and include fuel injection scheduling, rail pressure, air system actuator positions, and other boundary conditions applicable to the 4045 engine. While maintaining accuracy to the production engine, this model is not over-calibrated; it is capable of making valid predictions for steady-state and transient operating conditions.

The convective in-cylinder heat flux to the wall is given as

$$\dot{q}''=h\left(t_g-t_w\right) \quad (5)$$

where h is the heat transfer coefficient by the classical Woschni correlation with swirl term [28] (center swirl is about 1.4), t_g is the bulk gas temperature from the gas-phase thermodynamics solver, and t_w is the coated wall temperature [3]. It is possible that the heat transfer coefficient could be altered by the coated wall, but this effect was not included.

Wall Treatment Scenarios

In the following sections, two different heat flux treatments are examined. First, all combustion chamber surfaces are assumed to have the same wall architecture, referred to hereafter as the global heat flux method. Second, the heat flux is split into individual heat fluxes to the head (including intake/exhaust valves), piston and liner and, thus, each surface can become a unique multi-layer wall with different material characteristics.

Global Heat Flux

The current version of GT-Power (v2020 b2) [27] can only provide the total in-cylinder heat transfer rate $\dot{q}_{\text{global}}$ for each cylinder. The instantaneous heat flux $\dot{q}''_{\text{global}}$ is found as

$$\dot{q}''_{\text{global}}=\frac{\dot{q}_{\text{global}}}{A_{\text{total}}} \quad (6)$$

where A_{total} is the instantaneous in-cylinder surface area exposed to combustion gases. The resulting global heat flux is used to find the incremental step change, $\Delta\dot{q}''_{o,i}$ and convolved with the response function X as previously shown in Eq. 4 to

find the correct t_w for the next time step. For the *steady state* scenarios presented in this section, the coolant temperature was considered constant and, thus, it was superimposed and the second term of Eq. 4 was zero. Essentially, the steady state problem formulation is equivalent to the previous publication [3]. For the *drive cycle* the measured coolant temperature history was convolved with the response function Y to provide the contribution of the back-side wall to the full solution in Eq. (4).

Split Heat Flux Wall

The methodology presented in the previous section, *i.e.* global heat flux wall treatment, assumed that the combustion chamber consisted of a single multi-layer wall architecture. In this section, a methodology to allow splitting the global heat flux into individual heat fluxes to the head, piston and liner is developed. With the split heat flux methodology, one can use different wall thermal properties (and coatings) for each component.

In the current GT-Power version the individual-component heat fluxes can not be directly exported. The global heat transfer rate is the sum of the head, piston and liner heat transfer rates, such that

$$\dot{q}_{\text{global}} = \dot{q}''_{\text{head}} A_{\text{head}} + \dot{q}''_{\text{piston}} A_{\text{piston}} + \dot{q}''_{\text{liner}} A_{\text{liner}} \tag{7}$$

where $\dot{q}_{\text{global}}$ is the in-cylinder total heat transfer rate of each cylinder, which is provided by GT-Power for every time step and cylinder. The terms $\dot{q}''_{\text{head}}$, $\dot{q}''_{\text{piston}}$ and $\dot{q}''_{\text{liner}}$ are the head, piston and liner heat flux, respectively, and the terms A_{head}, A_{piston} and A_{liner} are the corresponding surface areas. The liner area varies with crank angle while the rest remain constant.

Convective heat transfer is assumed for each of the surfaces, such that

$$\dot{q}''_{\text{head}} = \hat{h}\left(t_g - t_{\text{w,head}}\right) \tag{8}$$

$$\dot{q}''_{\text{piston}} = \hat{h}\left(t_g - t_{\text{w,piston}}\right) \tag{9}$$

$$\dot{q}''_{\text{liner}} = \hat{h}\left(t_g - t_{\text{w,liner}}\right) \tag{10}$$

where $\hat{h}$ is a modified heat transfer coefficient to match total in-cylinder heat loss. By solving for $\hat{h}$

$$\hat{h} = \frac{\dot{q}_{\text{global}}}{t_{\text{gas}} A_{\text{total}} - \left(t_{\text{w,head}} A_{\text{head}} + t_{\text{w,piston}} A_{\text{piston}} + t_{\text{w,liner}} A_{\text{liner}}\right)} \tag{11}$$

one can use Eq. (8), (9) and (10) to get the individual head, piston and liner heat fluxes. Attention should be given to the denominator of Eq. (11) to avoid singularities. The back-side boundary condition is treated similarly as described earlier, with the only difference being that the head/liner and piston are exposed to coolant and oil, respectively.

The default GT-Power explicit time step was used for the flow calculations (pipe flows and in-cylinder combustion flows). Python user-defined function was called every 100μs to compute the coated wall surface temperature. The X and Y response functions are fully calculated only once at time equal zero, since they depend only on material properties and thickness of each layer. A finite impulse response time is chosen, based on tolerance criteria, for computational efficiency purposes. The instantaneous surface area is computed with respect to the piston position which is followed by the heat flux calculation as shown in Eq. (6) or Eqs. (8) to (10) for each time step and cylinder. Each wall temperature output is used as input to the cylinder objects that in turn calculate the heat fluxes of the next time step.

FIGURE 2 Steady state coated wall surface temperature as a function of crank-angle for the low-speed/medium-load engine condition for the baseline stock wall and various other coating architectures using the global wall heat flux treatment.

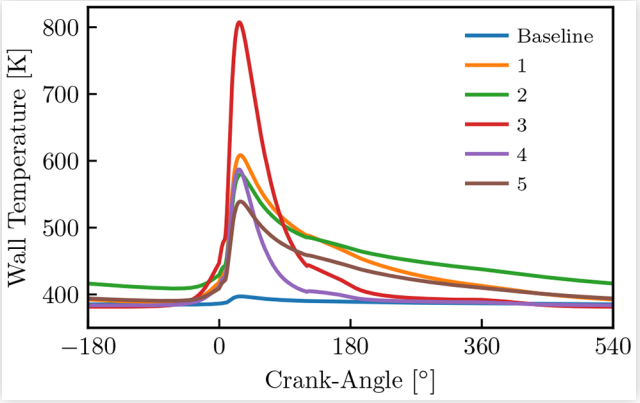

Steady State Analysis

Coating performance was evaluated for two conditions of the John Deere 4045 speed-load map. The first was a low-speed/medium-load case that had a 10.9 bar IMEPg at 800 rpm. The second was a high-speed/low-load case that had a 2.7 bar IMEPg at 2400 rpm.

All of the simulations were performed for a constant value of *brake torque*. This control was achieved by adjusting the mass of fuel injected. Therefore, one must be careful when comparing the normalized results that are presented because the normalization has been calculated using the case-specific mass of fuel.

The steady-state coated wall surface temperatures for the low-speed/medium-load case are shown as a function of crank-angle, in Fig. 2, for each of the six unique engine wall architectures using the global wall treatment described above. The material properties of each coating can be found in Table 2. Numerical values of wall surface temperature swing and the gas-exchange (EVO-IVC) cycle-mean temperature are given in Table 5 in the Appendix.

The stock power cylinder wall consists of three parts (head/piston/liner) with different material properties and thicknesses. An area-average technique based on the individual area and thickness of each component was used to estimate the stock "global wall" properties, shown in Table 2 as *Baseline*.

In Fig. 2, the baseline (blue) stock engine wall has almost negligible surface temperature variation during the cycle (≈10 K) while the five coated cases wall surface temperatures swing substantially throughout the cycle. Most of the coated wall structures have a surface temperature swing in the 150

TABLE 2 Thermal properties of wall architectures investigated.

Wall structure	Layer	k [W/m-K]	$\rho c \times 10^{-6}$ [J/m^3-K]	L [μm]
Baseline	global wall	85	3.8	9000
	head	26	4.5	10000
	piston	123	2.6	8600
	liner	45	3.9	6800
#1, ref. [12]	top	0.65	1.3	180
	bond	4.2	3.1	70
	global wall	85	3.8	8750
#2, ref. [13]	top	0.77	1.8	210
	gradient	0.85	1.5	70
	bond	4.07	0.9	70
	global wall	85	3.8	8650
#3, ref. [14]	top	0.35	0.4	100
	global wall	85	3.8	8900
#4, ref. [16]	top	0.67	1.3	65
	global wall	85	3.8	8935
#5, ref. [19]	top	0.85	2.3	180
	global wall	85	3.8	8820

FIGURE 3 Steady state surface heat flux as a function of crank-angle for the low-speed/medium-load engine condition for the baseline stock wall and various other coating architectures using the global wall heat flux treatment.

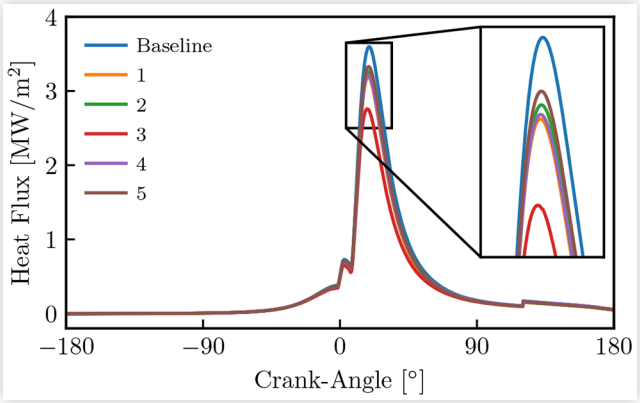

to 220 K range. Coating #1 has higher a temperature swing than coating #2, but the latter tends to retain heat throughout the cycle leading to higher wall temperatures during the exhaust, intake and compression strokes.

Coating #3 provided the highest temperature swing (≈ 430 K) among all the coatings selected from the modern literature. This coating also releases most of its thermal energy during the power stroke. During the exhaust stroke coating #3 tends to have the second to lowest temperature, with coating #4 being lowest. It important to note that there is a period where the trend reverses; during the first third of the intake stroke until the second third of the compression stroke coating #4 has the lowest wall temperature. This is a clear indication that less heat flows *from* the engine wall *to* the inducted air charge during the intake valve open period, improving volumetric efficiency.

FIGURE 4 Steady state coated wall surface temperature using coating #3 as a function of time for the low-speed cycle duration. The low-speed/medium-load and high-speed/low-load cases are compared for all four engine cylinders using the global wall heat flux treatment.

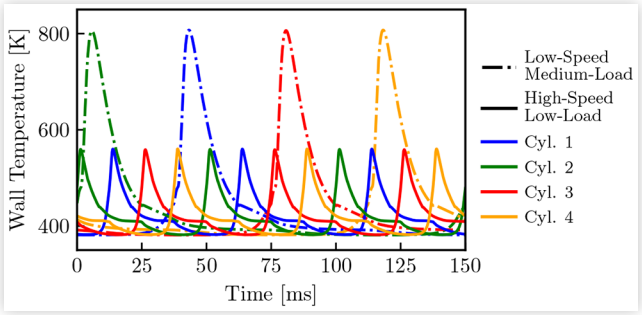

The Toyota SiRPA, coating #4, has almost the same temperature swing as coating #2, but its thermal properties led to much lower cycle-mean temperature during gas exchange. In addition, the SiRPA coating releases heat very quickly mostly due to the fact that it is the thinnest of all structures examined. Coating #5 showed the lowest temperature swing, but from the middle of the exhaust stroke to the end of compression stroke it closely matched coating #1.

The resulting surface heat flux for each coating architecture is shown in Fig. 3. The highest peak flux is observed from the baseline case and the lowest from coating #3. It is worth noting that coatings #1 and #4 have notably different wall temperature histories throughout the cycle in Fig. 2, yet their heat flux traces in Fig. 3 match closely for this low-speed/medium-load condition. Numerical values of peak surface heat flux and integrated heat transfer are given in Table 5 in the Appendix.

The wall temperature swing is a strong function of engine condition. A simple example is shown in Fig. 4 for coating #3. The low-speed/medium-load and high-speed/low-load wall temperatures are compared for all four cylinders for the duration of a 800rpm cycle. The high-speed/low-load case has a much smaller temperature swing than the low-speed/medium-load condition mostly due to the reduced time for heat transfer and lower fuel energy provided.

The split heat flux methodology was also investigated using the steady-state approach. An example of the individual

TABLE 3 Baseline data for the global and split heat flux wall treatment

	Low-Speed Medium-Load		High-Speed Low-Load	
	Global	Split	Global	Split
BSFC [g/kW-hr]	219.8	220.1	2098	2045
Fuel mass [mg/cyc]	273.94	274.00	73.25	71.33
Heat Transfer [kW]	21.93	21.93	18.06	16.72
Fuel Power [kW]	77.79	77.81	62.44	60.80
Brake Power [kW]	29.89	29.89	2.51	2.51
Exhaust Loss [kW]	17.69	17.92	25.32	25.61
Other [kW]	30.48	30.26	34.82	32.89

FIGURE 5 Steady state coated wall surface temperature of stock head, coated piston and stock liner for cylinder 1 at the low-speed/medium-load engine condition of coating #1. Material properties can be found in Table 2.

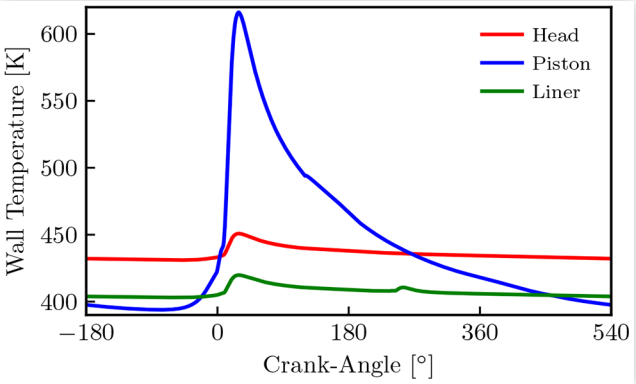

combustion chamber surface temperatures for cylinder 1 is shown in Fig. 5. Instead of using a single set of material properties (as was previously done for the global wall), the split heat flux methodology allows each surface to have its own properties. The stock power cylinder material properties can be found in Table 2. Only the piston was coated with coating #1, see Table 2. Compression ratio remained fixed in this analysis by removing the total coating's thickness from that of the stock piston.

The head, piston, and liner surface temperatures are shown in Fig. 5 as a function of crank angle. As expected there is a mean temperature difference between the three different surfaces, with the coated piston showing the most intra-cycle variation. The head and liner have very small temperature variation throughout the cycle (≈20 K). The coated piston temperature swing (≈220 K) is similar to that observed for the global case in Fig. 2.

To get a crude evaluation of coating performance under steady state operation, a system-level analysis was performed for the low-speed/medium-load and high-speed/low-load engine conditions. The former is a relatively high efficiency point, while the latter is a poor efficiency point since the engine makes almost no brake torque (≈10Nm). The fuel mass per cycle, in-cylinder heat transfer and exhaust loss are compared using the global wall heat flux method, and the split heat flux method where only the piston was coated. The baseline condition performance metrics for the global and split heat flux wall treatments can be found in Table 3, and the coated results measured relative to these baseline values are shown in Fig. 6 with their numerical values given in Table 6 of the Appendix.

In-cylinder heat transfer was reduced for all of the coatings studied, as shown in Fig. 6. The largest in-cylinder heat transfer reduction (17%) was seen using coating #3 with the full chamber coated at the low-speed/medium load condition. This coating generates the largest temperature swing and minimum peak heat flux, as shown earlier in Fig. 2 and 3 or Table 5. For this condition the heat transfer benefit reduces by half when only the piston is coated, see Fig. 6.

The fuel mass per cycle data show that a savings is predicted for all the global wall calculations. Coating #3 provides the highest fuel savings (4.5%) for the low-speed/medium-load case. Reducing the coated area to just the piston, the effect is reduced four-fold to 1.2%. However, the results for just coating the piston indicate cases where there is no effect (coating #4) or a slight increase in fuel consumption (coating #5).

The exhaust loss, *i.e.* exhaust sensible enthalpy, was found to increase for all of the coatings. This is noteworthy because, as mentioned above, the normalization was performed using the baseline data. Thus, using the global wall treatment for coating #3 as an example, there is an increase of exhaust enthalpy in spite of nearly 5% less fuel going into the engine. The global wall treatment, as expected, shows a larger effect than just the coated pistons. A maximum exhaust loss increase of about 6% is achieved in the high-speed/low-load case from coating #2, but the effect reduces by 4× when only the piston surface is coated. Coating #2 releases the heat slowly, and thus has increased wall surface temperature as can be seen in Fig. 2 or by comparing the cycle-mean wall temperatures during gas-exchange (EVO-IVC) in Table 5.

The steady-state results provide a mixed picture of the coatings' performance. The fuel mass per cycle *savings* for the split case (only piston coated) wall treatment is in the best case one half the global prediction and in one case there is actually a reversal of sign, *i.e.*, the piston-coated case used more fuel. Additionally, for the two operating conditions explored, the predicted fuel consumption benefit can vary by a factor of two. All of these results are explained by the complicated nonlinear coupling between the multiple effects at play. Therefore, in order to provide a comprehensive comparison between an uncoated and a coated engine the full drive cycle needs to be considered.

Drive Cycle Analysis

A brief review of the NRTC drive cycle is given first, followed by the implementation of experimental boundary conditions. A total of six drive cycle simulations were performed. Results are presented for stock baseline and two different coated wall architectures (coating #2 and #3) for a fully coated (global heat flux scenario) and piston-coated (split heat flux scenario) setup, integrated over the full drive cycle.

Drive Cycle Boundary Condition Specifications

The Non-Road Transient Cycle (NRTC) is an international transient certification cycle used to assess non-road engine vehicle performance, fuel consumption and emissions. The dynamometer transient driving schedule lasts ≈20 minutes with normalized speed and brake torque set points, with an average speed of 68% and average load of 39%, as shown in Fig. 7. Official certification involves running an NRTC from cold start, followed by a 20-minute soak period, and finally an NRTC from hot start. The hot NRTC is considered here to evaluate performance and fuel consumption. Pollutant emissions were not considered.

The drive cycle was run experimentally and the data were recorded to be used as boundary conditions in GT-Power. The engine speed, brake torque, common rail pressure, exhaust throttle and EGR valve angles, and fluid temperatures (coolant,

FIGURE 6 Fuel mass, in-cylinder heat transfer, and exhaust loss changes relative to the baseline results given in Table 3. The coating architectures are given in Table 2.

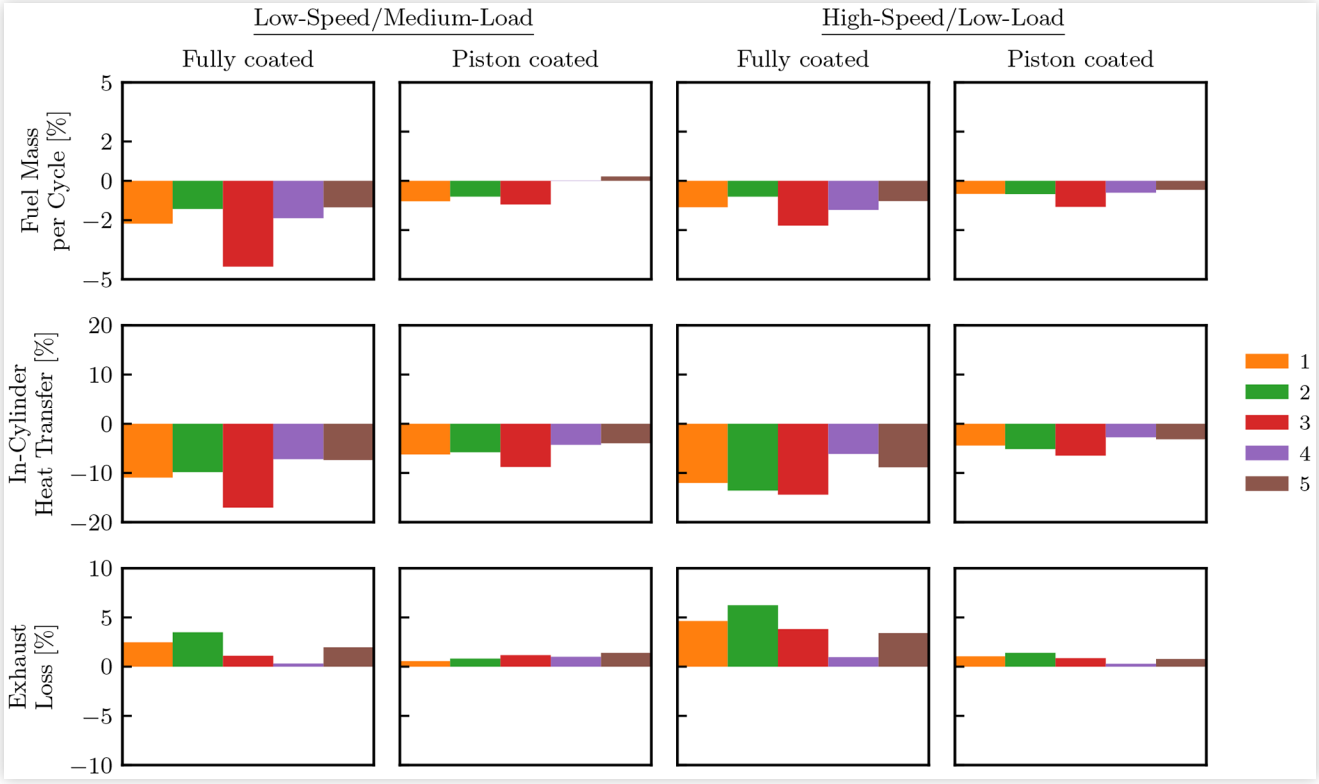

oil, intercooler and ambient), are shown in Fig. 7, and were imposed for all the transient cases. The coolant and oil temperature histories were particularly useful for the heat conduction analysis, as they are related directly with Eq. (4).

The drive cycle simulations were performed using a torque controller so that the brake power was constant for all simulations but the mass of fuel varied. The same treatment was performed for the steady state results. The comparison of global quantities based on normalized results, which used the baseline conditions as the reference, need to consider the reduction of fuel mass as appropriate.

Drive Cycle Results - Global Heat Flux

The wall surface temperature (top) and heat flux (bottom) are shown for three wall architectures (baseline, coating #2 and coating #3) and all four engine cylinders, in Fig. 8, over the full drive cycle using the global heat flux wall treatment. During the first 5 minutes of the baseline case (top left), the cycle-mean wall temperature increases due to both the coolant temperature increase, see Fig. 7, and the thermal energy that is absorbed. The surface temperature behavior differs significantly for the two coated cases. Coating #2 gives roughly half of the temperature swing achieved by coating #3, and the low-temperature envelope for coating #2 is higher than for coating #3 suggesting a lower volumetric efficiency.

The coatings' thermal performance, via the heat flux, is also shown in Fig. 8. The highest heat flux is observed for the baseline case. Coating #2 shows a reduced peak heat flux, and an even larger reduction is achieved with coating #3.

The time window from 11-13 minute is interesting. During this time, as seen from the expanded view in Fig. 9, the engine speed first ramps up from 2000 rpm to 2400 rpm and is held there. During the speed ramp the load is decreased at a slower rate from 340 N-m to 280 N-m, then starting from the 12th minute load suddenly drops to 60 N-m and then ramps back up to 220 N-m at steady speed. During the speed ramp both coatings show a small decrease in the surface temperature swing (part of which is attributed to the slightly decreased load), and the minimum surface temperature during gas exchange is slightly increased. This speed change is relatively small, but the observed effect of engine speed on coating performance is consistent with literature [2]. At higher speeds, there is less time available to absorb thermal energy in the coating and then released it back to the gas. An inherent difference is seen between the two coatings during the step load change and ramp in the latter part of the time window of Fig. 9. For coating #2 the minimum surface temperature shows a significant reduction (note the relevant reference to measure against is the intake air temperature) when the load decreases. In contrast, for coating #3 the minimum (gas exchange) surface temperature is relatively unaffected because of the low thermal inertia of the coating.

FIGURE 7 Engine dynamometer transient driving schedule (engine speed and brake torque) and recorded experimental data (rail pressure, exhaust throttle and EGR valve angle, and oil, coolant, intercooler and ambient temperature) of a Non-Road Transient Cycle (NRTC). The experimental data were used as boundary conditions to a fully calibrated system-level simulation.

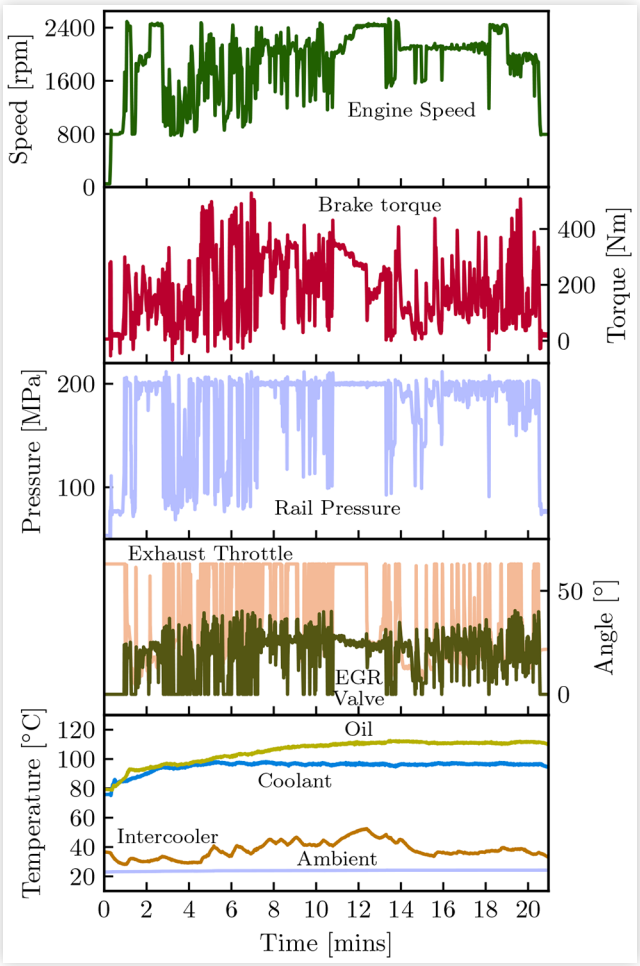

Drive Cycle Results - Split Heat Flux

The temporal evolution of the stock head, coated piston (coating #3) and stock liner wall surface temperature over the full drive cycle are presented in Fig. 10. The coated piston has the highest temperature and temperature swing among the components. The stock head and liner may have similar thermal properties, see Table 2, but their large temperature difference is attributed to the difference in thickness; the head is thicker hence has more thermal resistance. Additionally, the liner is coolest because of its variable surface area exposure; when the heat flux is at maximum during combustion the liner surface area is near its minimum value.

The integrated transient energy balance is shown in Fig. 11 for the baseline global heat flux case. The integrated results of the baseline for both global and split heat flux wall treatment, are given in Table 4. The sum of all terms in Table 4

FIGURE 8 Wall temperature (top) and heat flux (bottom) temporal evolution during a NRTC drive cycle for all four cylinders and combustion chamber wall architectures starting from left: baseline, coating #2 and coating #3.

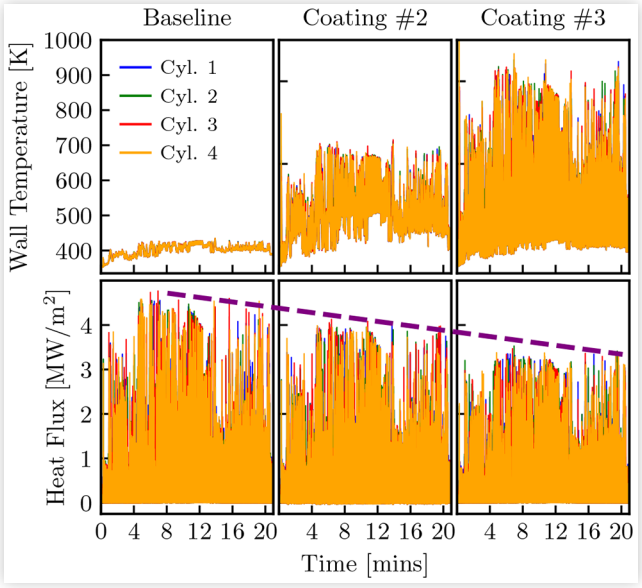

FIGURE 9 Expanded view of coating #2 and coating #3 wall surface temperature (top) and speed/load curve (bottom) temporal evolution during the 11th and 13th minute of the NRTC drive cycle for all engine cylinders.

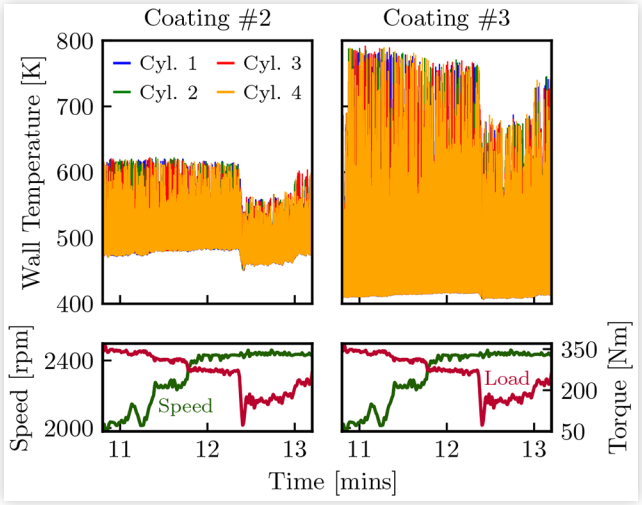

is the instantaneous fuel energy consumed over the drive cycle. *Brake* work is the integral of the average engine crankshaft brake power. *In-Cylinder Heat* energy is the integrated in-cylinder heat transfer for all four cylinders. *Exhaust* energy refers to the integrated exhaust sensible enthalpy. Finally, the term *Other* is attributed to any other energy pathway *e.g.*, heat transfer to EGR cooler, charge air cooler, heat rejection to coolant/oil in the cylinder head, and heat transfer to surroundings from the block/manifolds/turbine/pipes. It is interesting to note that the baseline total fuel mass is nearly identical for the global and split treatments.

FIGURE 10 Stock head, coated piston and stock liner wall temperature temporal evolution over NRTC drive cycle using the split heat flux wall treatment. Material properties of coating #3 used on top of the stock piston wall can be found in Table 2.

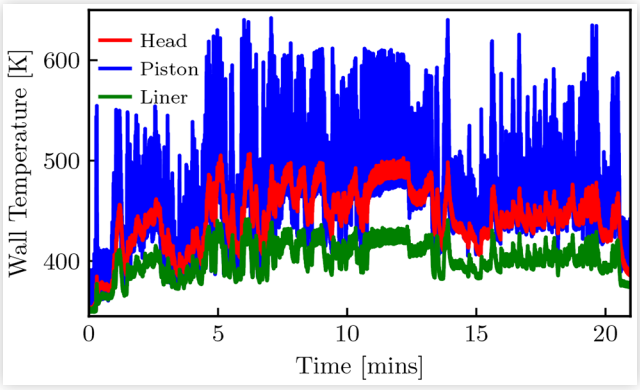

TABLE 4 Baseline energy balance breakdown and total fuel mass shown for the global and split heat flux wall treatment over the full NRTC drive cycle.

	NRTC Drive Cycle	
	Global	Split
Brake Work [MJ]	47.67	47.67
In-Cylinder Heat Transfer [MJ]	31.06	30.35
Exhaust Loss [MJ]	38.59	39.17
Other [MJ]	24.39	23.96
Total Fuel mass [kg]	3.325	3.311

In Fig. 12, the relative changes in integrated fuel mass and in-cylinder heat transfer, exhaust loss and other losses are presented for the global and split wall heat flux treatment of coatings #2 and #3. The tabulated data are given in Table 7. Note that the integrated brake power remained fixed for all the cases tested.

A maximum in-cylinder heat transfer reduction of 18.5% is recorded for coating #3 with a fully coated chamber.

FIGURE 11 Temporal evolution of the integrated energy over the NRTC drive cycle for the baseline John Deere 4045 engine using the global heat flux wall treatment.

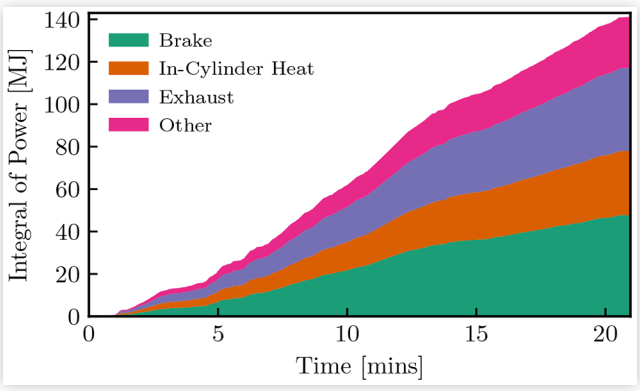

FIGURE 12 Relative changes (relative to baseline in Table 4) of fuel mass and integrated powers for coatings #2 and #3 using the global and split wall heat flux treatment over the duration of a full NRTC drive cycle. For numerical values see Table 7.

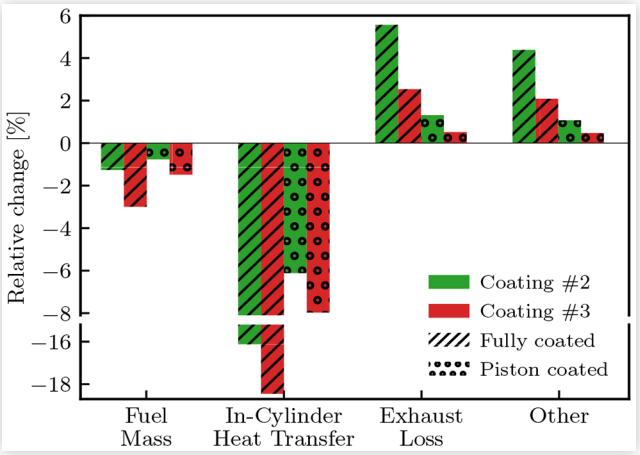

Limiting the coating to just the piston surface reduces the heat transfer benefit nearly 40%. The low-volumetric heat capacity and thickness of coating #3 absorbs heat quickly during the power stroke and releases it during the expansion and gas-exchange times.

A total fuel mass savings of 3% (≈100 gr) was predicted from coating #3 with the global wall treatment, but the effect drops to 1.5% when only the piston is coated. Coating #3 is predicted to reduce fuel mass more than coating #2. This trend is consistent with the steady state results given above, but no quantitative comparison can be given because it will depend strongly on the steady state conditions chosen for comparison.

The exhaust loss was predicted to be highest for coating #2 with the fully coated chamber. This 6% increase in exhaust heat loss corresponds to about a 10 K increase in drive-cycle-mean turbine outlet temperature. It is important to note that this temperature increase might seem small, but there 1.27% less fuel energy put into the engine during the drive cycle time. If that energy would have been provided, the exhaust enthalpy would have been even higher. The other losses scale directly with exhaust loss, as one would expect.

The piston-coated scenario is the most likely for practical application, and will be the basis for this brief summary of the coatings' effects during a complete drive cycle evaluation. Both coatings were effective at reducing in-cylinder heat transfer, with a substantial reduction predicted (6 or 8% depending on the coating). This effect should be considered an upper limit as there is some evidence that the surface roughness of the coating may adversely affect the local conditions. The reduction in heat loss to the combustion chamber surface did not result in a commensurate reduction in fuel consumed. There was a predicted reduction in fuel consumption (0.78% or 1.49% depending on coating - some of the benefit was directly recouped) but there was also an increase in the exhaust enthalpy and other losses, *i.e.*, the energy not lost to the combustion chamber surfaces is redistributed in many ways. The normalization scheme employed

underestimates these effects; the increase in exhaust enthalpy, for example, would be larger when calculated with a fuel energy normalization scheme. The overall effect of a thermal barrier coating, however, is that there is predicted to be a reduction in fuel consumed and an increase in exhaust gas temperature, which may be useful for exhaust aftertreatment considerations.

Conclusions

The analytical method to predict surface wall temperature of multi-layer thermal barrier coated walls, based on the solution methodology of [2, 3], was implemented in a commercial system-level simulation software package. The wall temperature at each time step was calculated by convolving the engine wall response function with the time-varying surface boundary condition, *i.e.*, in-cylinder heat flux and coolant temperature. The wall response function depends only on material properties and thickness of each layer and therefore can be computed once *a priori*. The convolution process is computationally efficient.

Two different wall heat flux treatment scenarios were investigated. The global heat flux scenario assumes that the combustion chamber has uniform wall properties while the split heat flux scenario allows the head/piston/liner to have unique thermal characteristics and therefore unique wall temperatures.

A fully calibrated production engine model was coupled with this tool to evaluate the performance of five modern, engine-specific coatings selected from the literature that have been tested experimentally.

The steady-state results revealed an engine-condition dependence and provided a mixed picture of the coatings' performance. A fully coated chamber, as expected, showed more promising results than reducing the coated area to just the piston. Under fixed brake torque conditions, all coatings (global or piston-coated) reduced in-cylinder heat transfer, but that did not guarantee a reduction in fuel consumption. Furthermore, all coatings resulted in higher exhaust enthalpy even though less fuel was injected. The predicted exhaust losses were higher by two-to-four times for the fully coated chamber scenario than for the piston-only coating scenario. The fuel savings were found to vary by a factor of two, depending on operating condition.

Experimental drive cycle data along with ECU data were used as boundary conditions in the model to simulate the full NRTC drive cycle. Two coating structures were chosen for analysis. Both coatings predicted a significant reduction of in-cylinder heat transfer, which led to a reduction in fuel consumption. The reduction in fuel consumption only accounted for a fraction of the reduced energy loss due to heat transfer. The exhaust enthalpy was found to increase by 0.5%, even though less fuel mass was consumed when coatings were present. For the likely scenario of a coated piston, one may expect to see up to a 1.5% reduction in fuel consumption and a corresponding brake specific CO_2 reduction over the drive cycle, depending on the coating architecture. The coated-wall thermal insulating properties provided higher wall surface temperature and thus lower heat transfer energy across the drive cycle, altering the engine performance. Lower heat transfer led to increased gas temperature and thus increased cylinder pressure during the expansion stroke. Right before the beginning of the intake stroke, the wall had already released heat efficiently and the surface temperature was close to the inducted air, minimizing the negative heat transfer which in turn led to higher volumetric efficiency than coating #2. The same amount of work was achieved with less injected fuel. The drive cycle showed 5-15% (relative) additional fuel savings and a 10% (relative) larger in-cylinder heat transfer reduction when compared to the steady state conditions examined.

References

1. Uchida, N., "A Review of Thermal Barrier Coatings for Improvement in Thermal Efficiency of Both Gasoline and Diesel Reciprocating Engines," *International Journal of Engine Research*, 2020.
2. Koutsakis, G., Nellis, G.F., and Ghandhi, J.B., "Surface Temperature of a Multi-Layer Thermal Barrier Coated Wall Subject to an Unsteady Heat Flux," *International Journal of Heat and Mass Transfer* 155, 2020.
3. Koutsakis, G. and Ghandhi, J.B., "An Analytical Approach for Calculating Instantaneous Multilayer-Coated Wall Surface Temperature in an Engine," *SAE International Journal of Advances and Current Practices in Mobility* 2:1303-1313, 2020.
4. Saputo, J.C., Smith, G.M., Lee, H., Sampath, S. et al., "Thermal Swing Evaluation of Thermal Barrier Coatings for Diesel Engines," *Journal of Thermal Spray Technology* 1-15, 2020.
5. Andruskiewicz, P., Najt, P., Durrett, R., Biesboer, S. et al., "Analysis of the Effects of Wall Temperature Swing on Reciprocating Internal Combustion Engine Processes," *International Journal of Engine Research*, 2017.
6. Caputo, S., Millo, F., Boccardo, G., Piano, A. et al., "Numerical and Experimental Investigation of a Piston Thermal Barrier Coating for an Automotive Diesel Engine Application," *Applied Thermal Engineering*, 2019.
7. Kosaka, H., Wakisaka, Y., Nomura, Y., Hotta, Y. et al., "Concept of "Temperature Swing Heat Insulation" in Combustion Chamber Walls, and Appropriate Thermo-Physical Properties for Heat Insulation Coat," *SAE International Journal of Engines* 6(1):142-149, 2013.
8. Kawaguchi, A., Iguma, H., Yamashita, H., Takada, N. et al., "Thermo-Swing Wall Insulation Technology; - A Novel Heat Loss Reduction Approach on Engine Combustion Chamber," *SAE Technical Paper Series*, 2016.
9. Broatch, A., Olmeda, P., Margot, X., and Gomez-Soriano, J., "A One-Dimensional Modeling Study on the Effect of Advanced Insulation Coatings on Internal Combustion Engine Efficiency," *International Journal of Engine Research*, 2020.
10. Taibani, A., Visaria, M., Phalke, V., Alankar, A., and Krishnan, S., "Analysis of Temperature Swing Thermal

Insulation for Performance Improvement of Diesel Engines," *SAE International Journal of Engines* 12(2):117-128, 2019.

11. Wakisaka, Y., Inayoshi, M., Fukui, K., Kosaka, H. et al., "Reduction of Heat Loss and Improvement of Thermal Efficiency by Application of "Temperature Swing" Insulation to Direct-Injection Diesel Engines," *SAE International Journal of Engines* 9(3):1449-1459, 2016.
12. Filipi, Z., Hoffman, M., O'Donnell, R., Powell, T. et al., "Enhancing the Efficiency Benefit of Thermal Barrier Coatings for Homogeneous Charge Compression Ignition Engines through Application of a Low-k Oxide," *International Journal of Engine Research*, 2020.
13. Gingrich, E., Tess, M., Korivi, V., Schihl, P., and Saputo, J., et al., "The Impact of Piston Thermal Barrier Coating Roughness on High-Load Diesel Operation," *International Journal of Engine Research*, 2019.
14. Andrie, M., Kokjohn, S., Paliwal, S., Kamo, L.S. et al., "Low Heat Capacitance Thermal Barrier Coatings for Internal Combustion Engines," *SAE Technical Paper Series* 1:1-13, 2019.
15. Andrie, M.J., Kamo, L., and Kamo, A., "Thermal Barrier Coatings Containing Aluminosilicate Particles," US Patent App, 16/036,364, 2020.
16. Kawaguchi, A., Wakisaka, Y., Nishikawa, N., and Kosaka, H., et al., "Thermo-Swing Insulation to Reduce Heat Loss from the Combustion Chamber Wall of a Diesel Engine," *International Journal of Engine Research*, 2019.
17. European Commission Horizon 2020, "EAGLE Project," GA No. 724084, 2020.
18. Chérel, J., Zaccardi, J.-M., Bouteiller, B., and Allimant, A., "Experimental Assessment of New Insulation Coatings for Lean Burn Spark-Ignited Engines," *Oil & Gas Science and Technology-Revue d'IFP Energies nouvelles* 75:11, 2020.
19. Bouteiller, B., Allimant, A., Zaccardi, J.-M., and Cherel, J., "New Ceramic Thermal Barrier Coatings Development in a Spark-Ignition Engine - Experimental Investigation," in *International Thermal Spray Conference*, Yokohama, Japan, ASM International, 2019.
20. Tsutsumi, Y., Nomura, K., and Nakamura, N., "Effect of Mirror-Finished Combustion Chamber on Heat Loss," SAE Technical Papers 902141, 1990, https://doi.org/10.4271/902141.
21. Powell, T., "Impacts of Thermal Barrier Coating Morphology and Catalytic Properties on Low Temperature Combustion Engine In-Cylinder Processes," PhD Thesis, Clemson University, 2018.
22. Powell, T., O'Donnell, R., Hoffman, M., Filipi, Z. et al., "Experimental Investigation of the Relationship between Thermal Barrier Coating Structured Porosity and Homogeneous Charge Compression Ignition Engine Combustion," *International Journal of Engine Research*, 2019.
23. Somhorst, J., Oevermann, M., Bovo, M., and Denbratt, I., "Evaluation of Thermal Barrier Coatings and Surface Roughness in a Single-Cylinder Light-Duty Diesel Engine," *International Journal of Engine Research*, 2019.
24. Keskinen, K., Vera-Tudela, W., Wright, M., and Boulouchos, K., "Experimental Investigation of Wall Heat Transfer Due to Spray Combustion in a High Pressure/High Temperature Vessel," in *THIESEL*, 2020.
25. Kogo, T., Hamamura, Y., Nakatani, K., Toda, T. et al., "High Efficiency Diesel Engine with Low Heat Loss Combustion Concept - Toyota's Inline 4-Cylinder 2.8-Liter ESTEC 1GD-FTV Engine," SAE Technical Paper 2016-01-0658, 2016, https://doi.org/10.4271/2016-01-0658.
26. Memme, S. and Wallace, J.S., "The Influence of Thermal Barrier Coating Surface Roughness on Spark-Ignition Engine Performance and Emissions," in *Internal Combustion Engine Division Fall Technical Conference*, American Society of Mechanical Engineers, Vol. 55096, pp. 893-905, 2012.
27. Gamma Technologies, *GT-SUITE* (Westmont, IL, 2020).
28. Heywood, J.B., *Internal Combustion Engine Fundamentals* (McGraw-Hill, 1988).

Contact Information

G. Koutsakis,
Engine Research Center
University of Wisconsin-Madison
koutsakis@wisc.edu

Acknowledgments

Support for this work was provided by Deere & Company.

Definitions, Acronyms, Abbreviations

$\dot{q}''$ - Heat Flux [Wm^{-2}]

h - Heat transfer coefficient [$Wm^{-2}K^{-1}$]

t - Temperature [K]

$\boldsymbol{\theta}$ - Time [s]

$\boldsymbol{X}$ - Response function of combustion surface due to heat flux changes [m^2KW^{-1}]

$\boldsymbol{Y}$ - Response function of back-side surface due to temperature changes [m^2KW^{-1}]

$\boldsymbol{k}$ - Thermal conductivity [$Wm^{-1}K^{-1}$]

$\boldsymbol{\rho}$ - Density [kgm^{-3}]

c - Specific heat capacity [$Jkg^{-1}K^{-1}$]

$\boldsymbol{\rho c}$ - Volumetric heat capacity [$Jm^{-3}K^{-1}$]

x - Distance [m]

L - Length [m]

Subscripts

g - gas

w - wall

o - combustion surface

N - back-side surface

i, n - time step index

Abbreviations

TBC - Thermal Barrier Coating

NRTC - Non-Road Transient Cycle

CI - Compression Ignition
EGR - Exhaust Gas Recirculation
GdZr - Gadolinium Zirconate
HCCI - Homogeneous Charge Compression Ignition
CO - Carbon Monoxide
CO_2 - Carbon Dioxide
uHC - unburned Hydrocarbon
YSZ - Yttria Stabilized Zirconia
SiRPA - Silica Reinforced Porous Aluminum
HVLP - High Volume Low Pressure
CFD - Computational Fluid Dynamics
TDC - Top Dead Center
BDC - Bottom Dead Center
IVC - Intake Valve Closing
EVO - Exhaust Valve Opening
DI - Direct Injection
ECU - Electronic Control Unit
IMEPg - gross Indicated Mean Effective Pressure
Ra - absolute profile height arithmetic average over length

Appendix

TABLE 5 Wall surface temperature swing, integrated wall temperature mean during gas-exchange (EVO-IVC), peak heat flux and integrated heat transfer are reported for all wall architectures using the global wall heat flux treatment for the low-speed/medium-load engine operating condition.

Wall	Temperature Swing [K]	Average wall temperature during gas-exchange (EVO-IVC) [K]	Peak Heat Flux [MW/m²]	Integrated Heat Transfer [kJ]
Baseline	12.5	387	3.6	21.93
1	220	422	3.19	19.53
2	171	442	3.26	19.77
3	426	395	2.76	18.19
4	203	389	3.21	20.35
5	149	415	3.33	20.31

The changes relative to the baselines (global or split wall heat flux treatment) in Table 6 were calculated for every performance metric as:

$$\%\text{change} = 100 \times \frac{\text{Coated} - \text{Uncoated}}{\text{Uncoated}} \tag{12}$$

TABLE 6 Engine performance metrics change in [%] basis relative to the baseline for all coatings using the global and split heat flux wall treatment for the low-speed/medium-load and high-speed/low-load steady state condition.

	Low-Speed/Medium-Load									
	Fully coated					Piston coated				
Coating	#1	#2	#3	#4	#5	#1	#2	#3	#4	#5
Fuel mass	−2.17	−1.42	−4.36	−1.90	−1.34	−1.04	−0.80	−1.20	−0.01	0.22
In-Cylinder Heat	−10.94	−9.82	−17.03	−7.19	−7.38	−6.24	−5.79	−8.79	−4.28	−3.96
Exhaust Loss	2.47	3.50	1.11	0.31	1.96	0.56	0.81	1.17	1.00	1.40
	High−Speed/Low−Load									
	Fully coated					Piston coated				
Coating	#1	#2	#3	#4	#5	#1	#2	#3	#4	#5
Fuel mass	−1.34	−0.80	−2.27	−1.48	−1.03	−0.66	−0.67	−1.32	−0.60	−0.45
In-Cylinder Heat	−12.04	−13.58	−14.40	−6.13	−8.84	−4.43	−5.15	−6.47	−2.75	−3.15
Exhaust Loss	4.64	6.24	3.82	0.97	3.41	1.05	1.41	0.86	0.29	0.78

TABLE 7 Engine performance metrics change in [%] basis relative to the baseline for coating #2 and #3 using the global and split heat flux wall treatment over a full NRTC drive cycle.

	Drive Cycle			
	Fully coated		Piston coated	
Coating	#2	#3	#2	#3
Fuel mass [%]	−1.27	−2.99	−0.77	−1.49
In-Cylinder Heat [%]	−16.14	−18.45	−6.12	−7.97
Exhaust Loss [%]	5.56	2.54	1.31	0.52
Other [%]	4.38	2.09	1.08	0.48

ISSN 0148-7191